

## Improved determination of the classical sphaleron transition rate

*J. Ambjørn*<sup>1</sup> and *A. Krasnitz*<sup>2</sup>

The Niels Bohr Institute,  
Blegdamsvej 17,  
DK-2100 Copenhagen Ø, Denmark.

### Abstract

We determine the sphaleron transition rate using real time lattice simulations of the classical system. An improved definition of the lattice topological charge allows us to obtain a more reliable estimate of the transition rate. For an SU(2) Yang-Mills-Higgs system in the broken phase we find the transition rate to be strongly suppressed, and we have observed no sphaleron transitions in the range of coupling constants used. For a pure SU(2) Yang-Mills system in large volumes the rate behaves as  $\kappa(\alpha_w T)^4$ , with  $\kappa$  slightly decreasing as the lattice spacing is reduced. If the lattice size is reduced to about twice the magnetic screening length, the rate is suppressed by finite-size effects, and  $\kappa$  is approximately proportional to the lattice spacing. Our rate measurements are supplemented by analysis of gauge field correlation functions in the Coulomb gauge.

*PACS:* 11.15.Ha, 12.38.Mh, 05.20.Gg, 05.40.+j.

*Keywords:* sphalerons; baryon asymmetry; lattice simulations; magnetic mass.

---

<sup>1</sup>E-mail: ambjorn@nbi.dk

<sup>2</sup>E-mail: krasnitz@nbi.dk

# 1 Introduction

Knowledge of the high-temperature baryon-number violation rate in the electroweak theory may be a key to origins of baryon matter. For temperatures close to and above the electroweak phase transition this essentially nonperturbative quantity can only be determined under two simplifying assumptions that (a) fermion degrees of freedom can be taken into account through modification of coupling constants, and that (b) the classical approximation is valid. The rate is then found by numerically following the real-time evolution of the Chern-Simons number in the classical (lattice) cutoff theory. This line of research was initiated in [1], and the last two years have seen much numerical effort to improve the simulations, as well as theoretical examination of the simplifying assumptions (mostly the second one). In our large-scale numerical simulation of the SU(2) Yang-Mills theory [2] we found that, with the standard approximate discretization of topological charge density, the classical Chern-Simons number diffusion rate  $\Gamma$  is finite in the continuum limit:

$$\Gamma = \kappa (\alpha_w T)^4. \quad (1)$$

We also estimated the value of the dimensionless coefficient  $\kappa$  in front of the  $T^4$  law (1):  $\kappa = 1.09 \pm 0.05$ . Moore [17] employed a different method for numerical determination of  $\Gamma$ , and his results agreed with ours. Tang and Smit [4] measured  $\Gamma$  in the SU(2) Yang-Mills-Higgs theory. In the low-temperature Higgs phase of the theory  $\Gamma$  is theoretically expected to be suppressed by the Boltzmann factor of the sphaleron potential barrier [6], rendering Chern-Simons number diffusion inobservable in a realistic numerical simulation. Surprisingly, no such strong suppression was found in [4]. Even more dramatic deviation from the sphaleron regime was found by Moore and Turok, raising suspicion that the residual diffusion in the Higgs phase is an artifact of the classical lattice theory [7]. Arnold, Son and Yaffe [8] (ASY in the following), and later Arnold [9] further questioned the validity of the classical result for  $\Gamma$ , arguing that the classical  $\Gamma$  must be proportional to the lattice spacing and therefore vanish in the continuum limit. More recently, Moore and Turok [10], employing an improved definition of Chern-Simons number, found that the transition rate in the lower-temperature phase was zero within the measurement error, as expected from the sphaleron approximation. They also detected a dependence of the rate on the lattice spacing, but that dependence was considerably milder than the prediction [8, 9] and left ample room for the existence of continuum limit.

Our present work is an effort to further examine the classical result for  $\Gamma$  and to identify its dependence on the lattice discretization. Our new results show that, with the standard lattice definition of topological charge density, there are spurious contributions to  $\Gamma$ , directly related to the well-known difficulty with defining topological quantities in a compact lattice gauge theory. We introduce a new definition of the lattice topological charge, designed to strongly suppress these artifacts. With most of the artifacts removed,  $\Gamma$  is indeed inobservably low in the Higgs phase of the Yang-Mills-Higgs theory. In the pure Yang-Mills theory, the use of the standard definition of topological charge leads to a systematic error in  $\Gamma$ . Arnold, Son, and Yaffe conjectured that this systematic error

creates an illusion of a  $\kappa$  independent of the lattice spacing, while the correct lattice rate vanishes in the continuum limit. We do find a tendency of the rate to decrease with the lattice spacing, but this tendency does not appear to be strong enough to rule out the existence of the continuum limit. There is nevertheless one instance in which the rate exhibits proportionality to the lattice spacing in a wide range of the latter: the Yang-Mills theory in a small volume, where finite-size effects give rise to a sphaleron barrier. In that case, however, there remains a possibility that the continuum rate exists, but is very small due to an exponential suppression of barrier configurations.

The plan of this paper is as follows. We begin by explaining the cooling method for measuring lattice topological charge in Section 2. This method is used to place an upper bound on the rate in the low-temperature phase of the Yang-Mills-Higgs system (Section 3) and to estimate the rate in the large-volume limit of the Yang-Mills theory (Section 5). We also consider sphaleron transitions in the Yang-Mills theory in a small volume (Section 4). A closer look at the ASY scenario is taken in Section 6, where we study the dynamics of gauge fields in the Coulomb gauge. A discussion of the emerging picture is given in Section 7.

## 2 Cooling method for the lattice topological charge

Consider the standard lattice approximation for the topological charge per unit time

$$\dot{N}_{\text{CS}} = \frac{i}{32\pi^2} \sum_{j,n} (\bar{E}_{j,n}^\alpha + E_{j-n,n}^\alpha) \sum_{\square_{j,n}} \text{Tr} (U_{\square_{j,n}} \sigma^\alpha), \quad (2)$$

where

$$\bar{E}_{j,n}^\alpha \equiv \frac{1}{2} E_{j,n}^\beta \text{Tr} (\sigma^\alpha U_{j,n} \sigma^\beta U_{j,n}^\dagger).$$

Using the standard notation, we assign to every lattice site  $j$  link matrices  $U_{j,n}$  in the fundamental representation of  $\text{SU}(2)$  and lattice analogs of color electric fields  $E_{j,n}$ , three of each, corresponding to the three positive lattice directions  $n$ . The usual plaquette variable is denoted by  $U_{\square}$ , and  $\sigma^\alpha$  are the three Pauli matrices. In fact, it is misleading to write the left-hand side of (2) as a time derivative of  $N_{\text{CS}}$  or any other fixed-time functional of the fields: the object on the right-hand side of (2) is not a total time derivative (TTD). This shortcoming of the lattice topological charge density (TCD) is well known and related to the difficulty in defining on a lattice an analog of the continuum  $N_{\text{CS}}$  with the correct properties under gauge transformations [17]. Recently ASY [8] pointed out that deviations of the lattice topological charge per unit time from TTD may give rise to systematic errors in the transition rate. For smooth field configurations (2) tends to the continuum  $\dot{N}_{\text{CS}}$ . However, thermal field configurations on the lattice are not smooth, hence (2) does not approach a TTD in the continuum limit.

The idea behind the cooling method is to replace the real-time trajectory in the phase space (obtained by integrating the classical equations of motion) by another path between the same endpoints, the one along which phase-space configurations are predominantly

smooth. Lattice topological charge, computed along such a path using the naive definition (2), would suffer much less from systematic errors than the one computed along the real-time trajectory. We shall first present the method for a wide class of Hamiltonian systems and later discuss its application to topological transitions. A simplified version of the method was used in [11, 12] to study the time flow of eigenvalues of the (lattice) Dirac Hamiltonian in the presence of the time dependent gauge field generated by the real time, finite temperature simulations, and it was shown that the cooling strips off the high energy modes, while it does not affect the (long wave length) eigenvalue modes which cross zero and which are responsible for the change of baryon number. The results reported in [11] provided the first proof that the sphaleron-like transitions observed in the real time lattice simulations are indeed long wave length excitations and not lattice artifacts.

Let the real-time evolution of a dynamical system be described by a Hamiltonian depending on coordinates  $q_i$  and momenta  $p_i$  ( $i = 1, \dots, N$ ):  $H = \sum_i p_i^2/2 + V(q)$ . We introduce, along with the real time  $t$ , a cooling time  $\tau$ , of which all the dynamical variables are functions:  $p_i = p_i(t, \tau)$ ,  $q_i = q_i(t, \tau)$ . The  $t$  dynamics at  $\tau = 0$  is given by

$$\partial_t q_i(t, 0) = p_i(t, 0); \quad \partial_t p_i(t, 0) = -\partial_{q_i} V(q(t, 0)),$$

while the evolution in the  $\tau$  direction is an overdamped motion (cooling):

$$\partial_\tau q_i(t, \tau) = -\partial_{q_i} V(q(t, \tau)). \quad (3)$$

If we insist that the real-time equations for the coordinates  $\partial_t q_i(t, \tau) = p_i(t, \tau)$  hold everywhere in the  $t, \tau$  plane, then the  $\tau$  dependence of momenta, consistent with (3), is given by

$$\partial_\tau p_i(t, \tau) = -p_j(\tau) \partial_{q_i, q_j}^2 V(q(t, \tau)). \quad (4)$$

It is instructive to consider the  $\tau$  evolution described by (3)-(4) in the vicinity of a static solution  $\partial_{q_i} V = 0$ . The equations of motion (3)-(4) can be linearized and dynamical variables can be chosen as eigenmodes of these linearized equations:  $\partial_\tau q_i = -\omega_i^2 q_i$ ,  $\partial_\tau p_i = -\omega_i^2 p_i$ . Thus in the vicinity of a static solution cooling leads to an exponential decay of stable eigenmodes and exponential growth of unstable ones. Moreover, the rate of decay (growth) is especially rapid for high-frequency modes.

Suppose there is a coordinate (call it  $Q$ ) along which  $V$  is periodic. For simplicity we can assume that variations of  $Q$  are stable eigenmodes of the linearized equations of motion in the vicinity of periodic minima of  $V$  and the unstable ones in the vicinity of saddle points separating these minima. For sufficiently large  $\tau$   $Q(t, 0)$  will be mapped by cooling to  $Q(t, \tau)$  in a close vicinity of a minimum, unless  $Q(t, 0)$  lies close to a saddle point. As a result, if the  $Q(t, 0)$  motion consists of transitions between minima separated by fluctuations close to a minimum, the picture will sharpen under cooling: fluctuations of  $Q(t, \tau)$  near a minimum will have a smaller magnitude, whereas transitions between vacua (the time spent in the vicinity of a saddle point) will become shorter. If this indeed is the case for  $Q$ , two lessons can be learned. On the one hand, the average rate of transitions between minima for  $Q(t, \tau)$  should obviously be independent of  $\tau$ . On the

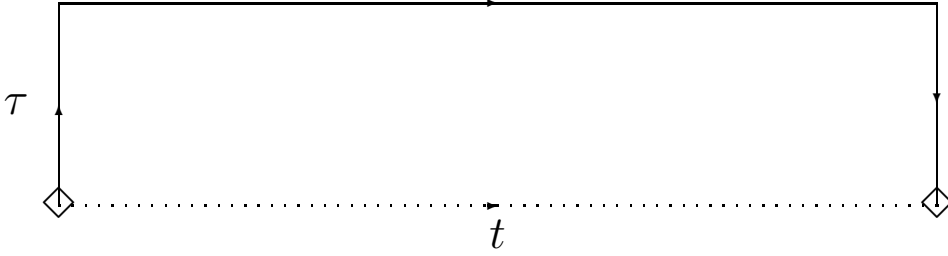


Figure 1: A  $\Pi$ -shaped trajectory in the  $t, \tau$  plain used for determination of topological charge with cooling. The endpoints of a  $\tau = 0$  real-time trajectory, shown by a dotted line, are denoted by diamonds.

other hand, care should be exercised if  $t$  is discretized for numerical purposes: for large  $\tau$  the transition times may become shorter than the  $t$  time step.

Consider now cooling as a method for approximating topological charge. Lattice topological charge per unit time is not a TTD. For smooth field configurations a lattice TCD can be expanded in powers of the lattice spacing, the leading term in the expansion being the continuum TCD. For a thermal field configuration this expansion is formal since in three dimensions thermal configurations are not smooth. By cooling, however, these configurations can be made smooth enough for the expansion to make sense. Then a lattice TCD will give rise to much smaller deviations from a TTD. We are therefore led to the following method of determining the topological charge. For any two instances of real time consider evolution of lattice fields along a  $\Pi$ -shaped trajectory in the  $t, \tau$  plain, with  $\tau$  sufficiently large to give a smooth cooled configuration, while, at the same time,  $\tau \ll t$ . Variation of topological charge with  $\tau$  is found by replacing  $t$  derivatives with  $\tau$  derivatives in the expression for TCD, whereas  $t$  derivatives at  $\tau \neq 0$ , required for the horizontal part of the trajectory, are found using (4). If the space integral of a lattice TCD were a TTD, the topological charge along any such trajectory would be independent of  $\tau$ . This is not the case for an approximate lattice TCD. However, for sufficiently deep cooling the topological charge becomes nearly independent of  $\tau$ . Indeed, deviations from a TTD are suppressed along the horizontal part of the trajectory. The vertical parts of the trajectory, where deviations from a TTD are not suppressed, are of a fixed (short) duration and give rise to a small error in determination of topological charge. Unlike in the  $\tau = 0$  case, this error does not accumulate. We now write down the cooling equations for the Yang-Mills theory described on the lattice by the Kogut-Susskind Hamiltonian

$$H_{YM} = \frac{1}{2} \sum_{j,n} E_{j,n}^\alpha E_{j,n}^\alpha + \sum_{\square} \left( 1 - \frac{1}{2} \text{Tr} U_{\square} \right).$$

In doing so it should be kept in mind that link matrices  $U$  are  $SU(2)$  group elements, each belonging to its own group. Hence the cooling equation for a link  $U$  can be written using covariant derivatives  $D^\alpha$  on the group to which  $U$  belongs:

$$\partial_\tau U = -D^\alpha H_{YM} D^\alpha U. \quad (5)$$

Here  $\alpha$  is an adjoint SU(2) index. If we choose to work with right covariant derivatives,  $D^\alpha U = -iU\sigma^\alpha$ . Since  $H_{YM}$  is linear in any given  $U$ ,  $D^\alpha H_{YM}$  is obtained by retaining of  $H_{YM}$  only terms proportional to  $U$ , with  $U$  replaced by  $D^\alpha U$ .

The cooling equations for the lattice electric fields  $E^\alpha$  are derived, in analogy with (4), by requiring, separately for each link, that the Hamiltonian equation of motion  $\dot{U} = -iU\sigma^\alpha E^\alpha$  holds everywhere in the  $t, \tau$  plane. Denoting  $E \equiv \sigma^\alpha E^\alpha$  we then obtain

$$\partial_\tau E = i\partial_\tau(U^\dagger \dot{U}) = (\partial_\tau U^\dagger)UE + iU^\dagger\{H_{YM}, \partial_\tau U\}, \quad (6)$$

where  $\{ \}$  are Poisson brackets and  $\partial_\tau U$  is substituted from (5) (we refrain here from writing the somewhat cumbersome explicit expression for  $\{H_{YM}, \partial_\tau U\}$ ).

The cooling method as described for the Yang-Mills theory applies essentially unchanged to the Yang-Mills-Higgs system whose Hamiltonian is

$$H_H = H_{YM} + \sum_j |\pi_j|^2 + \sum_{j,n} |\phi_{j+n} - U_{j,n}^\dagger \phi_j|^2 + \lambda \sum_j (|\phi_j|^2 - v^2)^2. \quad (7)$$

Our notation for the scalar fields is standard, *i.e.*, to every lattice site  $j$  we assign the scalar doublet  $\phi_j$  along with its conjugate momentum  $\pi_j$ . For the gauge fields one simply replaces  $H_{YM}$  by  $H_H$  in (5)-(6). These equations are complemented by the cooling equations for the scalar fields and momenta, which are a straightforward implementation of (3)-(4).

### 3 The rate in the Yang-Mills-Higgs theory

We used the cooling method in order to study the real-time evolution of Chern-Simons number in the SU(2) theory with and without the scalar field. In (7) we chose  $\lambda = 0.09109$ , corresponding to the tree-level  $m_H/m_W$  ratio of 0.423. Since the static properties of the classical theory closely resemble those of the dimensionally reduced one, we expected our lattice system to undergo a strongly first order phase transition. This is indeed what we find: the system exhibits a metastability at  $beta = 11.25$ , with an easily detectable latent heat and a large discontinuity in the conventionally used "string bit" order parameter

$$u \equiv \langle \phi_j^* U_{j,n} \phi_{j+n} / (|\phi_j^*| |\phi_{j+n}|)^{1/2} \rangle$$

as shown in Figure 2. Therefore, according to the conventional wisdom [13], the sphaleron regime should set in at temperatures immediately below the transition. At  $\beta = 12$  the sphaleron estimate for  $\Gamma$  involves the Boltzmann factor  $\exp(-\beta E_{\text{sph}})$  which prohibits direct observation of sphaleron transitions in a feasible numerical simulation.

Our numerical experiment at  $\beta = 12$  reveals a dramatic difference between the naive and refined definitions of topological charge (Figure 3). While the former is a random walk with deviations as large as 2 for a real-time trajectory of 2000 units, deviations of the latter never exceed 1. In fact, the motion of the refined Chern-Simons number

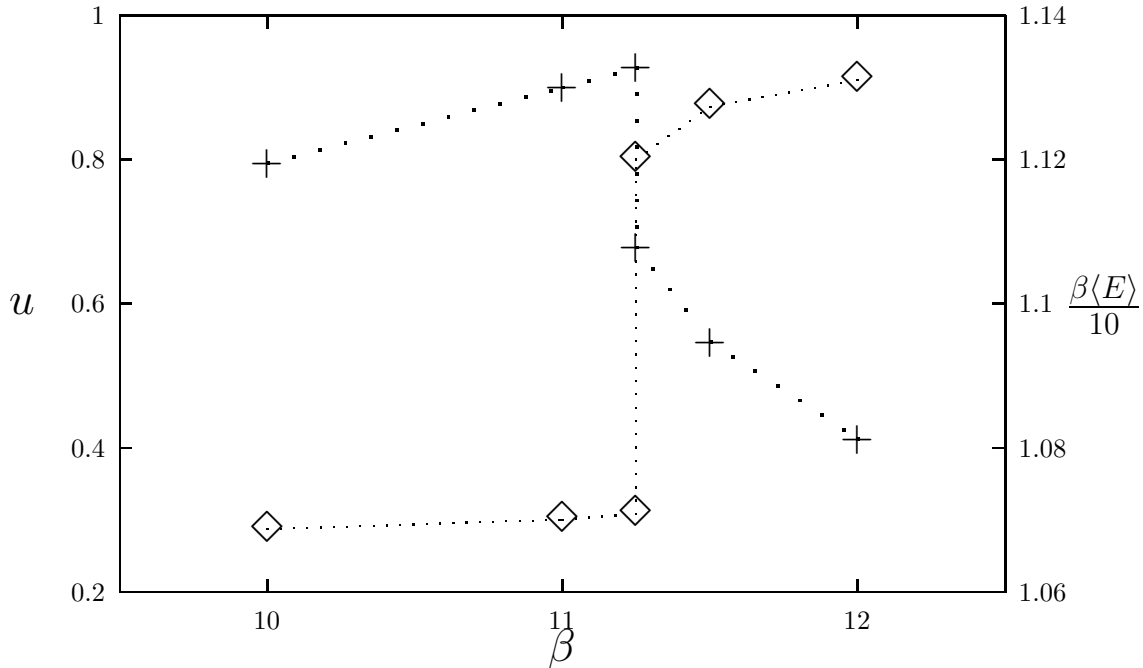


Figure 2: The "string bit" order parameter (diamonds) and the average energy per degree of freedom normalized by the energy of a free theory (pluses) for the Yang-Mills-Higgs theory with the tree-level  $m_H/m_W = 0.423$ . Note the discontinuity of both quantities at  $\beta = 11.25$ . The error bars are smaller than the plotting symbols. The dotted lines are to guide the eye.

is completely consistent with thermal fluctuations in the vicinity of one of the gauge-equivalent vacua and involves no diffusion between the vacua. In order to eliminate a possibility of diffusion with a time scale longer than 2000 units we followed the real-time evolution of the refined  $N_{CS}$  for  $2 \times 10^4$  time units. Again, we detected no sign of diffusion. Our results, together with observations of Ref. [7], strongly suggest that the slow diffusion of the naively defined Chern-Simons is spurious. Using the refined definition instead, we can place an upper bound on the sphaleron transition rate, expressed in terms of the dimensionless coefficient  $\kappa$ :  $\kappa = (\pi\beta)^4/(Vt) < 0.01$ , where  $Vt$  is the total space-time volume of our simulation. Clearly, this upper bound cannot be used to confront the sphaleron estimate which it exceeds by many orders of magnitude.

## 4 The rate in the Yang-Mills theory for small volumes

Since we suspect the naive definition of topological charge density to give rise to systematic errors in  $\Gamma$ , it is necessary to revise the results of [2] for the Yang-Mills theory, obtained using that definition. While our ultimate goal is to determine  $\Gamma$  for lattice

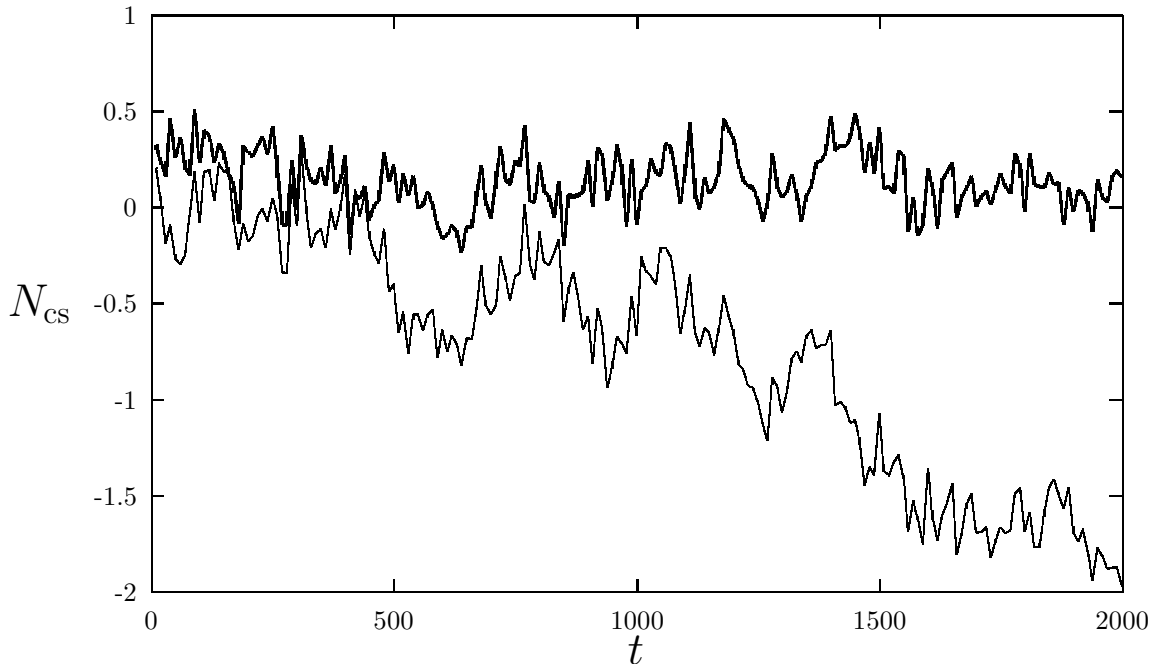


Figure 3: Time history of  $N_{\text{CS}}$  in the Yang-Mills-Higgs theory with (the upper curve) and without (the lower curve) the cooling improvement.

systems large enough to rule out finite-size effects, it is instructive to first consider smaller-volume systems. As we observed in [2], finite-size effects in  $\Gamma$  set in as soon as the linear size  $L$  of the lattice is close to the inverse temperature  $\beta$ . This phenomenon can be interpreted as follows. In the infinite-volume system there is no potential barrier separating topologically distinct vacua. Indeed, such a barrier is prohibited by the scale invariance of the classical theory. A finite size breaks the scale invariance and gives rise to the minimal barrier height of  $18.15/L$  for the periodic boundary conditions used here [18]. Making use of this property, we can suitably adjust the  $\beta/L$  ratio in order to study the  $N_{\text{CS}}$  behavior in the sphaleron regime. With this goal in mind, we performed a simulation at  $\beta/L = 1$ . As Figure 4 shows, motion of the naively defined  $N_{\text{CS}}$  can be seen as consisting of three components: thermal fluctuations, rapid transitions with a magnitude close to 1, and slow diffusion. If the refined definition is used, the slow diffusion component is absent from the  $N_{\text{CS}}$  time history. If we put this result together with our findings for the Yang-Mills-Higgs system, a consistent picture emerges: the true sphaleron transitions occur rapidly, while the slow diffusion of the naive  $N_{\text{CS}}$  is a discretization artifact.

Next, we determine the transition rate  $\Gamma$  in the small-volume case. This is most easily and efficiently done by counting the clearly distinguishable sphaleron transitions. The rate is then the number of transitions per unit volume per unit time. The advantage of this procedure over determining the rate as the  $N_{\text{CS}}$  diffusion constant is that the sphaleron event count is the same with either  $N_{\text{CS}}$  measurement method. We therefore



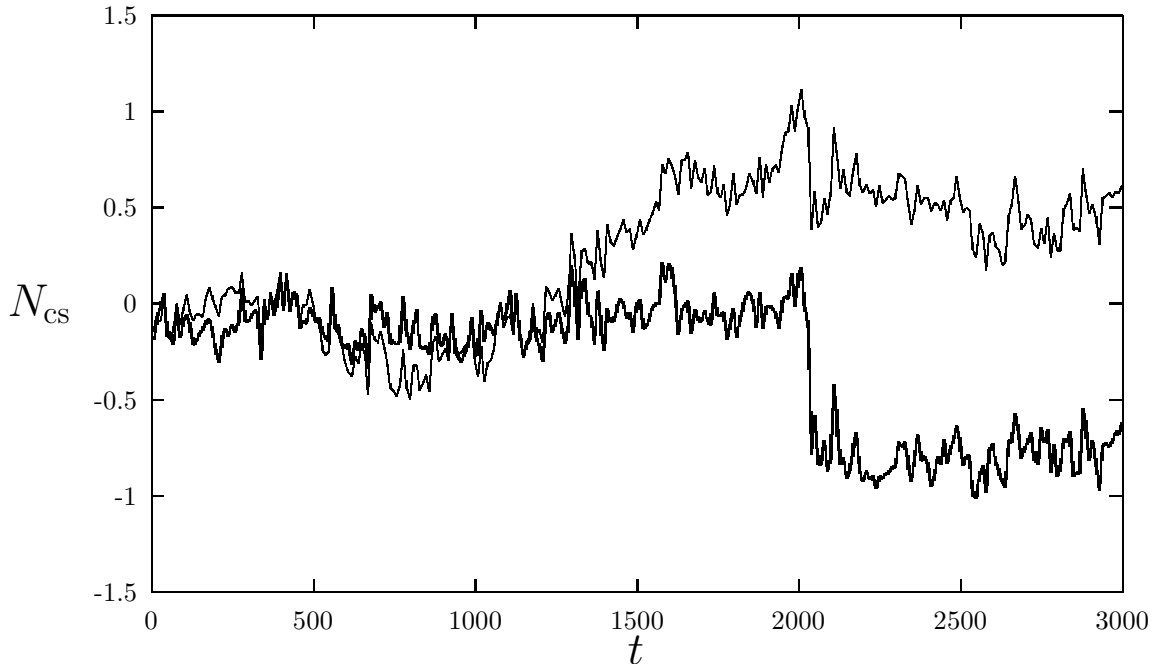


Figure 4: Time history of  $N_{\text{CS}}$  in the Yang-Mills and without the cooling improvement at  $\beta = L = 12$ . Both curves exhibit rapid fluctuations and a sphaleron transition at  $t \approx 2000$ , but, for the naive definition of  $N_{\text{CS}}$ , there also is a slow diffusion upwards.

$\beta = L$	10	12	14	16	20
events	111	109	113	73	50
time	$5.55 \times 10^5$	$8.2 \times 10^5$	$1.23 \times 10^6$	$1.02 \times 10^6$	$1.44 \times 10^6$
$\kappa$	$0.195 \pm 0.018$	$0.155 \pm 0.015$	$0.125 \pm 0.012$	$0.112 \pm 0.013$	$0.0676 \pm 0.0096$

Table 1: Effective  $\kappa$  for  $\beta/L = 1$ .

use the naive definition of  $N_{\text{CS}}$  in this part of the work.

We have observed between 50 and 100 events for  $\beta = L = 10, 12, 14, 16, 20$ . Since any two consecutive events are widely separated in time and unlikely to be correlated, we determine the rate with the relative accuracy  $n(\beta)^{-1/2}$ , where  $n(\beta)$  the total number of observed events for a given  $\beta$ . Our findings, summarized in Table 1, clearly show dependence of the effective  $\kappa$  on  $\beta$ , and hence on the lattice spacing. As can be seen in Figure 5, for  $10 \leq \beta \leq 16$  this dependence is consistent with  $\kappa \propto \beta^{-1}$ , but this simple proportionality cannot accommodate the  $\beta = 20$  point in a convincing way.

Clearly, our small-volume measurements fail to demonstrate the existence of continuum limit for the classical rate. Our simulations give support to ASY prediction  $\kappa \sim 1/\beta$  except maybe for the largest value of  $\beta$ . However, as we shall see in the following, a closer examination of the gauge field dynamics leaves room for alternative explanations of this discretization dependence of the small-volume rate.

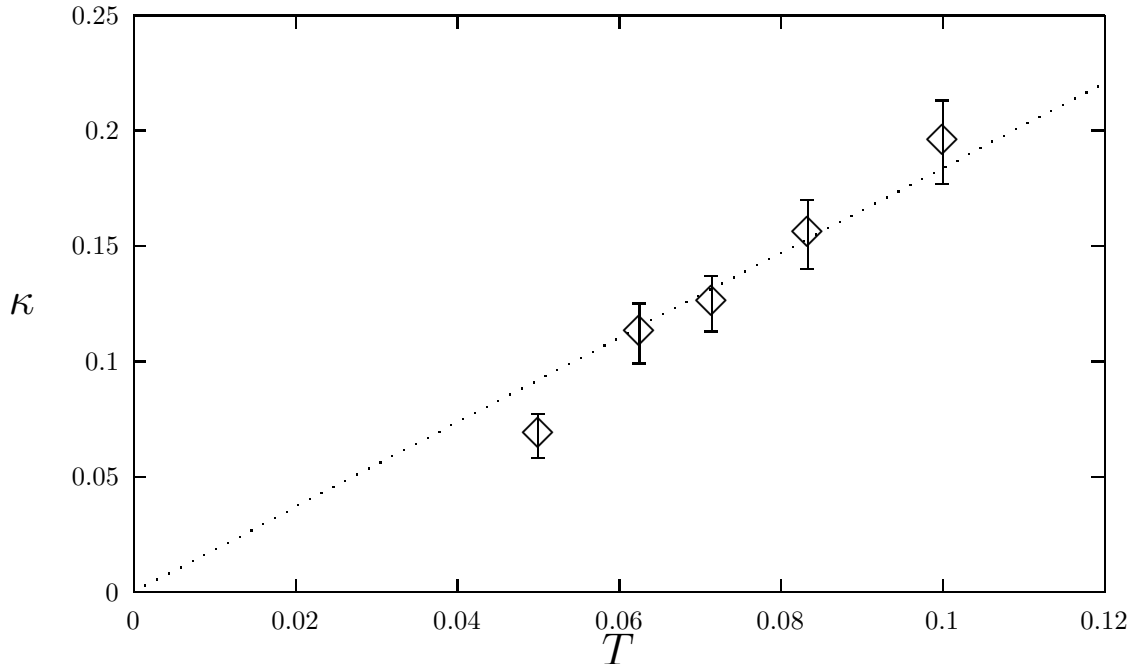


Figure 5: Effective  $\kappa$  as a function of  $T \equiv 1/\beta$  in the Yang-Mills theory for  $\beta = L$ . The dotted line is a linear fit through the origin using all the data except the  $\beta = 20$  point.

## 5 The large-volume rate in the Yang-Mills theory

In order to eliminate the systematic error in  $\Gamma$  resulting from the naive definition of topological charge we performed a series of large-volume simulations similar to the one reported in [2], but this time using the refined definition of  $N_{\text{CS}}$ . The cooling method is very costly computationally. For this reason we were unable to produce a measurement sample of the same size as in [2], with a comparable numerical effort. Our new results therefore contain larger statistical errors. In order to make use of the existing data from [2] we adopted the following procedure. Whatever definition of  $N_{\text{CS}}$  is used, the rate  $\Gamma$  is found by fitting the average squared topological charge  $\langle B^2(t) \rangle$  to a linear function of the time interval  $t$  in a suitable range of values of  $t$ . The rate is then the slope of that linear function. To rephrase, the rate can be determined given a numerical estimate for the joint probability distribution of  $D_i \equiv \langle B^2(t_i) \rangle$ , where  $t_i$  ( $1 \leq i \leq l$ ) is a discrete set of  $t$  values to be used in the fit. We assume this probability distribution to have the normal form

$$P(\{D\}) \propto \exp\left(-\frac{1}{2}(D_i - \bar{D}_i)(C^{-1})_{ij}(D_j - \bar{D}_j)\right), \quad (8)$$

where  $C$  is the estimated covariance matrix and  $\bar{D}_i$  is the estimate of  $D_i$  obtained by averaging over the data sample (*i.e.*,  $\bar{D}_i \rightarrow D_i$  with increasing measurement accuracy [15]). We shall take (8) to represent results of our high-statistics study [2]. In the current simulation we measure the improved topological charge  $B'(t)$  along with the naive one  $B(t)$ . We then find the corresponding  $\bar{D}_i$  and  $\bar{D}'_i$ , which we can jointly call  $\bar{\Delta}_j$ ,  $1 \leq j \leq 2l$ ,

$\beta$	$L$	length $\times$ number of trajectories	$\kappa$	biased $\kappa$
10	32	$2000 \times 20$	$1.48 \pm 0.08$	$1.44 \pm 0.03$
12	32	$2000 \times 20$	$1.36 \pm 0.09$	$1.39 \pm 0.06$
14	32	$2000 \times 10$	$1.33 \pm 0.12$	$1.38 \pm 0.10$
14	36	$1500 \times 20$	$1.27 \pm 0.15$	
16	36	$1500 \times 20$	$1.28 \pm 0.10$	

Table 2: Summary of the large-volume study of  $\kappa$  in the Yang-Mills theory.

meaning that  $\bar{\Delta}_j \equiv \bar{D}_j$  for  $j \leq l$  and that  $\bar{\Delta}_j \equiv \bar{D}'_{j+l}$  for  $j > l$ . We also estimate the covariance matrix  $\mathcal{C}$  for  $\{\bar{\Delta}\}$ , leading to the joint probability distribution  $\Pi$  for  $\{\Delta\}$  completely analogous to (8):

$$\Pi(\{D\}, \{D'\}) \propto \exp\left(-\frac{1}{2}(\Delta_i - \bar{\Delta}_i)(\mathcal{C}^{-1})_{ij}(\Delta_i - \bar{\Delta}_i)\right), \quad (9)$$

It is obvious that for a fixed set of  $\{D\}$  values of  $\{D'\}$ , averaged with the corresponding conditional probability, will be shifted away from  $\{\bar{D}'\}$  appearing in (9). This also holds true if the distribution (8) of  $\{D\}$  is given instead of a sharp set of values. We then average  $\Pi$  over  $\{D\}$  with the weight  $P$  to obtain the corrected distribution for  $\{D'\}$ :

$$P'(\{D'\}) = \int [dD] \Pi(\{D\}, \{D'\}) P(\{D\}). \quad (10)$$

We refrain from writing down the somewhat cumbersome result of the trivial Gaussian integration (10). It is clear that  $P'(\{D'\})$  is again a normal distribution, with corrections to both averages of  $D'_i$  and to their covariance matrix.

We now present results of our analysis. Table 2 summarizes the large-volume simulations we performed. Throughout the simulations the Hamiltonian time step was 0.05, and 5000 thermalization steps [3] were performed before every Hamiltonian trajectory. We used cooling depth  $\tau = 0.2$  for the improved determination of  $N_{CS}$ . Within our measurement accuracy further cooling made no difference in the rate. As in our previous work, squared topological charge for a given time interval was first averaged within every Hamiltonian trajectory, and these averages, assumed independent, served as an input for further statistical analysis, as described. While the dimensionless coefficient  $\kappa$  tends to decrease as a function of beta, our results cannot be said to favor the  $1/\beta$  behavior of  $\kappa$  advocated in Ref. [8].

## 6 Dynamics of gauge fields in the Coulomb gauge

We have seen in both large and small volumes the tendency of the rate to decrease as the continuum limit is approached. A decrease of  $\kappa$  as a function of  $\beta$  was advocated in Ref. [8]. In a nutshell, Ref. [8] argued as follows. Baryon-number violating processes mainly involve gauge fields with wavelengths  $\sim \beta$ , whose motion is overdamped due to

interaction with hard modes. This overdamping leads to a  $\beta^{-1}$  behavior of  $\kappa$ . While in the small-volume case we observed this behavior of  $\kappa$  in a range of values of  $\beta$ , the decrease in  $\kappa$  for large volumes was significantly slower than  $\sim 1/\beta$ . We therefore thought it useful to study the motion of the long-wavelength gauge fields in some detail.

Gauge fields can only be defined by choice of a gauge. In this work we chose the Coulomb gauge: on the one hand, it is often used in the relevant analytical work [19]; on the other hand, lattice gauge-fixing techniques have been developed for this gauge. The lattice Coulomb gauge condition is usually defined for every lattice site  $j$  in terms of  $A_{j,n} \equiv (1/(2i))(U_{j,n} - U_{j,n}^\dagger)$ :

$$\partial \dot{A}_j \equiv \sum_n (A_{j,n} - A_{j-n,n}) = 0, \quad (11)$$

where  $n$  denotes the three lattice directions. For the SU(2) group this condition can be obtained by extremizing

$$\text{Tr} \sum_{j,n} U_{j,n} \quad (12)$$

with respect to gauge transformations. This gauge is known to lead to Gribov copies; the unwanted copies are discarded by requiring the absolute maximum of (12). It is important to note that in a system with periodic boundary conditions (11) and (12) are preserved by global gauge transformations. This additional gauge freedom is not important as long as we only consider static properties of gauge fields, *e.g.*, screening correlation functions, but it must be removed if we wish to compare gauge fields at different instances of dynamical evolution. We do so by imposing two additional global conditions:

$$\text{Tr} \sigma^1 \sum_j A_{j,1} = \text{Tr} \sigma^2 \sum_j A_{j,1} = \text{Tr} \sigma^1 \sum_j A_{j,2} = 0.$$

In order to fix the gauge, we employed a combination of iterative overrelaxation and Fourier acceleration algorithms. The former was used to attain the accuracy of  $10^{-3}$  for  $\text{Tr}(\partial \dot{A})^2$  per site, and the latter to reduce  $\text{Tr}(\partial \dot{A})^2$  to below  $10^{-6}$ . We took Gribov copies into account by repeatedly performing first a random gauge transformation, then the Coulomb gauge fixing on the same field configuration, and choosing among the resulting gauge copies the one with the largest  $\text{Tr} \sum_{j,n} U_{j,n}$ . Within our measurement accuracy, this procedure had no effect on the observables.

We first determined the magnetic screening length from screening correlation functions of the form

$$G(z) \equiv \text{Tr} \sum_{z_0} \langle \bar{A}(z_0) \cdot \bar{A}(z_0 + z) \rangle, \quad (13)$$

where  $\bar{A}(z_0)$  is the average of  $A$  over the plane with one lattice coordinate fixed to  $z_0$ . We further average  $G(z)$  over the three directions of the displacement  $z$  (we will use the same notation for the average over directions). The magnetic mass is found by fitting  $G(z)$  to  $C \exp(-mL/2) \cosh(m(z - L/2))$ . The results for  $\beta = 10, 12, 14$  and  $L = 32$ , tabulated in Table 3, are accurately described by  $m = (2.630 \pm 0.005)/\beta$  in lattice units,

$\beta$	10	12	14
$m$	$0.27 \pm 0.02$	$0.23 \pm 0.01$	$0.184 \pm 0.006$
$m_D$	$0.712 \pm 0.025$	$0.69 \pm 0.04$	$0.68 \pm 0.04$

Table 3: Magnetic and Debye screening masses for the  $32^3$  classical system.

*i.e.*,  $m = (0.657 \pm 0.001)g^2T$  in the continuum notation. Thus we find that in the classical theory and in the range of temperatures considered  $m$  increases with  $g^2T$  steeper than  $0.466g^2T$  reported in Ref. [16] for the high-temperature quantum theory. In that work correlation functions were computed at much lower  $\beta \leq 3.47$  and in Landau, rather than Coulomb, gauge. Note, however, that both in Ref. [16] and in the current work  $G(z)$  could only be described by  $C \exp(-mL/2) \cosh(m(z - L/2))$  for  $z$  close to  $L/2$ , whereas for small values of  $z$  the decay of  $G(z)$  is noticeably slower. That is to say,  $1/m$  underestimates distances for which transverse gauge fields are strongly correlated in space.

Similarly, we estimated the Debye screening mass  $m_D$  from

$$G_D(z) \equiv \text{Tr} \sum_{z_0} \langle \overline{E}_z(z_0) \overline{E}_z(z_0 + z) \rangle, \quad (14)$$

where, *e.g.*,  $\overline{E}_z(z_0)$  denotes the average of the Cartesian  $z$  component of the lattice color electric field over the lattice plane whose  $z$  coordinate is  $z_0$ . We further average  $G_D$  over the three lattice directions and fit the result to  $C \exp(-m_D L/2) \cosh(m_D(z - L/2))$ , just as we did for the magnetic mass. The results are summarized in the bottom line of Table 3. Assuming  $m_D \propto 1/\sqrt{\beta}$ , our data is best described by  $m_D = (2.328 \pm 0.002)/\sqrt{\beta}$ , slightly above the perturbative estimate  $m_D = 2.01/\sqrt{\beta}$  [9]. Therefore for  $\beta \leq 14$   $m_D/m \leq 3.7$  in the classical theory, and these two scales are not completely separated. This point could be important for understanding our results for the rate.

Next, we consider the dynamical behavior of gauge fields in the Coulomb gauge. We determined real-time correlation functions of fields with a definite lattice momentum  $2\pi k/L$  in one of the three lattice directions, for  $0 \leq k \leq 4$ . More specifically, we studied

$$G(k, t) \equiv \text{Re} \langle A_{k,p}^*(t) A_{k,p}(0) \rangle,$$

where  $p$  runs over the two transverse polarizations. We further averaged  $G(k, t)$  over the three directions of  $k$ , and the notation  $G(k, t)$  is from now on used for that average. The resulting correlation functions, plotted in Figure 6, exhibit the following important features. First the motion of the gauge fields is clearly overdamped for  $k = 0, 1$ : the corresponding  $G(k, t)$  decay without oscillations. For  $k = 3, 4$  the field motion is underdamped, and an oscillatory behavior of  $G(k, t)$  is clearly observed. The  $k = 2$  case belongs to an intermediate regime, which, within our accuracy, we cannot classify as underdamped or overdamped.

Note that for  $k = 0, 1$  the  $G(k, t)/G(k, 0)$  against  $t/\beta^2$  curves coincide (within our measurement accuracy) for all three values of  $\beta$ . This coincidence, however, does not

hold for higher values of  $k$ . It appears that the higher the temperature, the higher is  $k$  at which the overdamping sets in. In the next section we confront these properties of the gauge field correlation functions with our rate measurements and with the ASY scenario.

There is no obvious way to compare our  $G(0,t)$  with the  $W$  real-time correlation function computed in Ref. [5] for the Yang-Mills-Higgs theory. In that work the  $k = 0$   $W$  decay rate was found to be very small and roughly proportional to  $1/\beta$  in the high-temperature phase. However, that result was obtained using local objects which only approximate gauge fields (in the unitary gauge) sufficiently deep inside the low-temperature phase.

## 7 Discussion

We now summarize our findings. We saw that, with the spurious  $N_{CS}$  diffusion removed by the cooling method, the sphaleron rate in the low-temperature phase of the Yang-Mills-Higgs theory is too low to be measured in the space-time volume attained in our simulations. The best we can do in this case is place an upper bound on the rate. That upper bound exceeds the analytical sphaleron prediction by many orders of magnitude and hence it is of limited value. The rate in the low-temperature phase close to the phase transition is a crucial parameter in any scenario of electroweak baryogenesis. Our results, as well as those by Moore and Turok [10], indicate that a straightforward real-time simulation may not be an adequate tool for finding this, very possibly extremely small, rate.

The focus of our numerical effort in this work is the approach of the classical rate to a continuum limit in the Yang-Mills theory. Our results for large volumes ( $L > 2\beta$ ) show that the dimensionless coefficient  $\kappa$  tends to decrease with the lattice spacing. This decrease, however, does not appear to be rapid enough to match the ASY scenario, in which overdamping of gauge fields at the magnetic length scale leads to the zero continuum limit for  $\kappa$ . In this respect our results are in a qualitative agreement with those of Moore and Turok [10], who used a different procedure for measuring topological charge. On the other hand, our values of  $\kappa$  are systematically lower than those of Moore and Turok, except for the point closest to the continuum limit,  $\beta = 16$ .

We observe a much stronger dependence of  $\kappa$  on the lattice spacing in the small-volume setting  $\beta = L$ . Over a range of values of  $\beta$ , this lattice spacing dependence is a simple proportionality.

Our measurements leave open three possibilities for the behavior of the transition rate close to the continuum limit.

1. The rate vanishes in the continuum limit, regardless of the lattice size to the magnetic screening length ratio. For small volumes this scenario is consistent with our observations. For large volumes, it can be reconciled with our data if a more rapid decrease in  $\kappa$  sets in at larger  $\beta$ .

2. Both the large-volume and the small-volume rates are finite in the continuum limit. This scenario is favored by our large-volume data. It could be that an asymptotic approach of the small-volume  $\kappa$  to the continuum limit occurs at  $\beta$  values larger than those considered here.
3. The large-volume rate remains finite, but the small-volume rate vanishes in the continuum limit<sup>3</sup>. This possibility is favored by our data.

Consider now the additional information on the gauge field dynamics obtained from the Coulomb-gauge correlation functions. As we have seen, motion of gauge fields with momenta 0 and  $2\pi/32$  is overdamped. A closer examination shows, however, that this is not quite the overdamping of long-wavelength modes predicted by ASY. Indeed the time scale for the correlation function decay is proportional to  $\beta^2$  for these wavelengths, if  $\beta$  is varied while keeping the wavelength *fixed*. ASY predict that the decay time at a *fixed* wavelength should behave as  $1/\beta$ . The decay times are short, of the order of several time units, *i.e.*, shorter than the corresponding wavelengths, whereas, in the ASY derivation, it is essential that the decay times be much longer than the wavelengths. Moreover, as our magnetic mass measurement shows, the overdamping only occurs for modes with wavelengths somewhat above the magnetic screening length. Harder modes, presumably corresponding to the magnetic scale, are not overdamped.

We can now discuss the three possibilities we have listed for the rate behavior in the continuum in the light of our knowledge of the gauge field dynamics in the Coulomb gauge. Consider sphaleron transitions in a small-volume Yang-Mills theory. With periodic boundary conditions, the sphaleron solution extends over the entire volume of the system [18]. Therefore it has a significant zero-momentum component of the gauge field whose motion is overdamped, with the decay time  $\sim \beta^2$  rather than  $\sim \beta = L$ . It is possible that this overdamping gives rise to the  $1/\beta$  behavior of  $\kappa$  in small volumes. On the other hand, it appears unlikely that very soft overdamped modes play a role in the  $N_{CS}$  diffusion in large volumes. Indeed, for our  $L = 32$  lattices, these modes correspond to excitations whose linear size is close to  $L$ . If these modes were important for formation of sphaleron-like configurations, we would expect a strong finite-size dependence of the rate. Such a dependence, however, is not observed (*cf* the  $\beta = 14$  rate for  $L = 32$  and for  $L = 36$ ). Hence the sphaleron-like transitions, whose spatial size is determined by the magnetic mass, should not be strongly affected by damping of these soft modes. Modes with momenta on the magnetic scale or harder are not overdamped. Thus it appears that the ASY mechanism does not operate in topology-changing processes in our large-volume simulations.

The argument just given supports the third possibility on our list. That possibility, however, is quite unusual: it requires that  $\kappa$  vanishes above some critical value of  $\beta/L$ . A way to avoid this situation could be as follows. Topology-changing transitions in

---

<sup>3</sup>It seems very likely that  $\kappa$  is a growing function of the volume. Thus we discard here yet another possibility, whereby the large-volume rate vanishes in the continuum, but the small-volume one remains finite.

small volumes could proceed through barrier configurations whose size is considerably smaller than  $L$ . These configurations need not have overdamped Fourier components. Indeed, all but the constant modes on our  $\beta = L$  lattices are not overdamped. These smaller barrier configurations are stronger suppressed by Boltzmann factors than the sphaleron, but that does not necessarily preclude their finite contribution to the rate in the continuum. That continuum,  $\beta$ -independent  $\kappa$  might be so small that, in the range of  $\beta$  values considered,  $\kappa$  is still dominated by the  $1/\beta$  term. This is a way in which the second possibility on our list may be realized.

Finally, the first possibility on our list cannot be ruled out. While it is not favored by our data, the case may be otherwise in a weaker-coupling regime. In the current work the Debye to magnetic mass ratio is below 3.7, so these two scales may not be completely separated. It may be necessary to further increase  $\beta$  in order to reach the range of validity of perturbation theory on which the ASY scenario is substantially based. Since  $m/m_D$  only decreases as  $1/\sqrt{\beta}$ , while the rate decreases at least as rapidly as  $1/\beta^4$ , exploring couplings much weaker than those presently considered is likely to be computationally costly.

## Acknowledgments

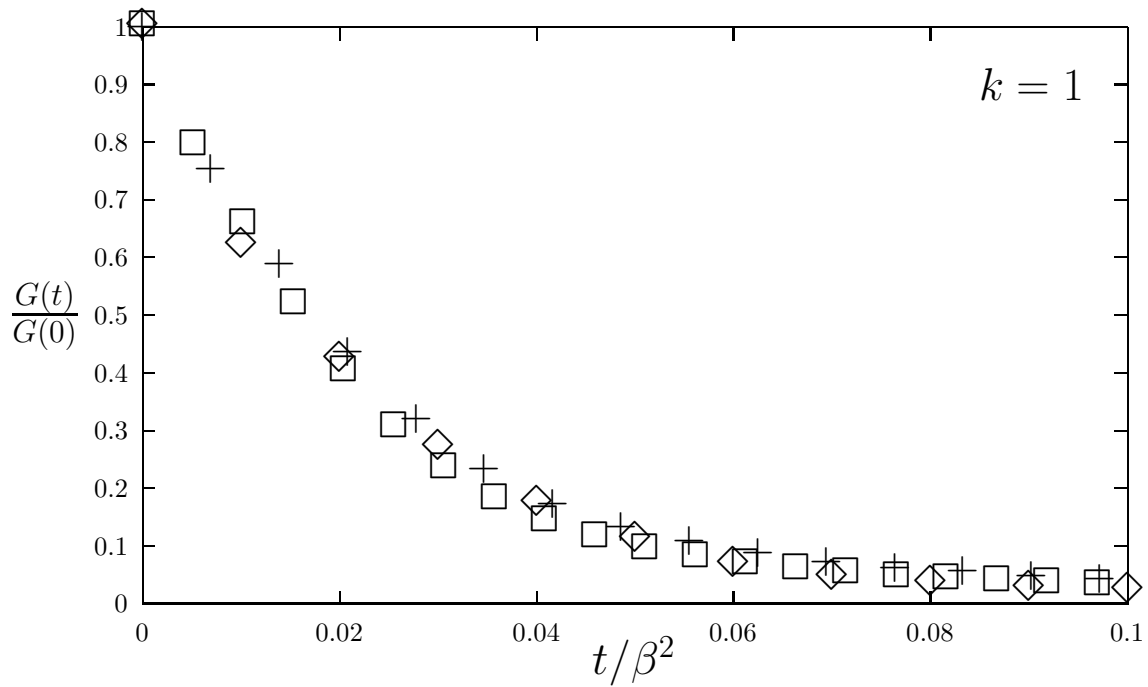
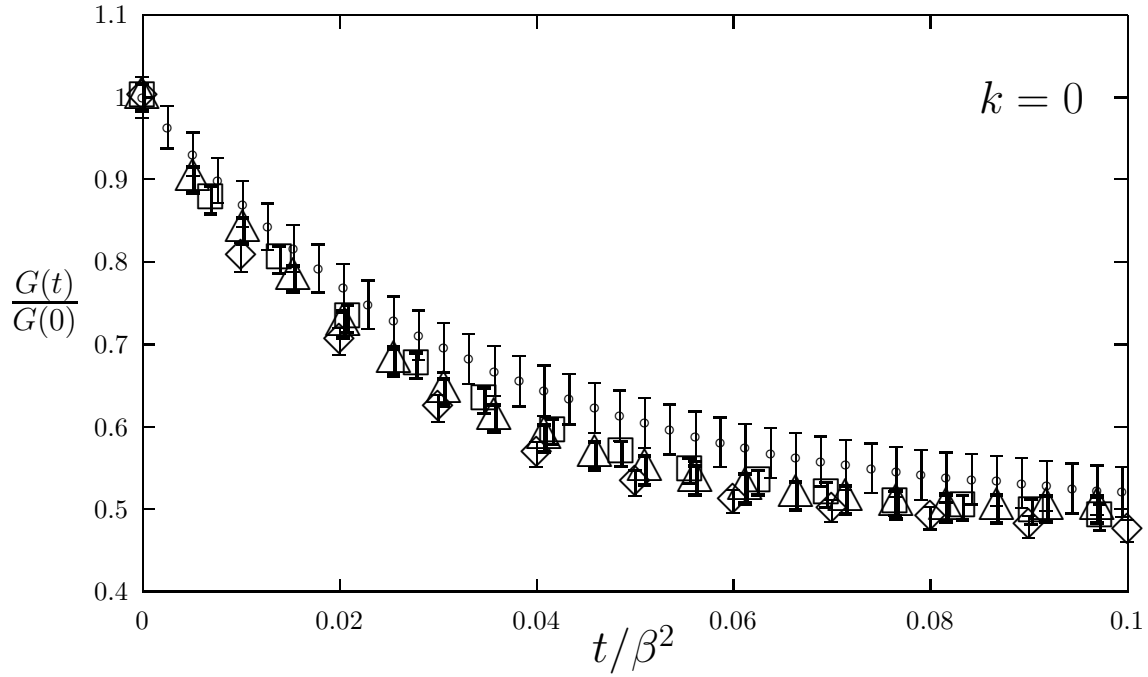
We are indebted to L. McLerran and R. Venugopalan for illuminating discussions. Thanks are due to G.D. Moore, J. Smit, and M.E. Shaposhnikov for useful comments. We also are grateful to Arnold, Son and Yaffe and to G.D. Moore and N. Turok for communicating their results to us prior to publication; to U.M. Heller, J. Rank, J. Hetrick and S. Gottlieb for advice and help with Fourier-accelerated gauge fixing. Parallel implementation of algorithms used in this work is based on software developed by the MILC collaboration [20]. Numerical simulations reported in this work were performed on the SP/2 massively parallel computer at the UNI-C.

## References

- [1] J. Ambjørn, T. Askgaard, H. Porter and M.E. Shaposhnikov, Phys. Lett. **B244** (1990) 479; Nucl.Phys. **B353** (1991) 346.
- [2] J. Ambjørn and A. Krasnitz, Phys. Lett. **B362** (1995) 97.
- [3] A. Krasnitz, Nucl. Phys. **B455** (1995) 320.
- [4] W.-H. Tang and J. Smit, Nucl. Phys. **B482** (1996) 265.
- [5] W.-H. Tang and J. Smit, *Numerical study of plasmon properties in the SU(2) Higgs model*, University of Amsterdam report ITFA-97-02, hep-lat/9702017 (1997).
- [6] P. Arnold and L. McLerran, Phys. Rev. **D36** (1987) 581.



- [7] G.D. Moore and N. Turok, Phys. Rev.**D55** (1997) 6538.
- [8] P. Arnold, D. Son and L.G. Yaffe, Phys. Rev.**D55** (1997) 6264.
- [9] P. Arnold, *Hot B violation, the lattice, and hard thermal loops*. University of Washington report UW-PT-97-2, hep-ph/9701393.
- [10] G. D. Moore and N. Turok, *Lattice Chern-Simons number without ultraviolet problems*. Princeton University report PUPT-1681, hep-ph/9703266.
- [11] J. Ambjørn and K. Farakos, Phys. Lett. **B294** (1992) 248.
- [12] J. Ambjørn, K. Farakos, S. Hands, G. Koutsoumbas and G. Thorleifsson, Nucl. Phys. **B425** (1994) 39.
- [13] For a recent review, see V.A. Rubakov and M.E. Shaposhnikov, Phys. Usp. **39** (1996) 461.
- [14] M. Garcia Perez, and P. van Baal, Nucl. Phys. **B468** (1996) 277.
- [15] This procedure is routinely used for, *e.g.*, extracting particle properties from propagators, as described in detail in S. Gottlieb, W. Liu, R. Renken, R. Sugar, and D. Toussaint, Phys. Rev. **D38** (1988) 2245.
- [16] U.M. Heller, F. Karsch, and J. Rank, Phys. Lett. **B355** (1995) 511.
- [17] G.D. Moore, Nucl. Phys. **B480** (1996) 657.
- [18] M. Garcia Perez, P. van Baal, Nucl.Phys. **B429** (1994) 451,  
P. van Baal and N.D. Hari Dass, Nucl. Phys. **B385** (1992) 185.
- [19] E. Braaten and R.D. Pisarski, Phys. Rev. **D42** (1990) 2156.
- [20] C. Bernard, T. DeGrand, C. DeTar, S. Gottlieb, A. Krasnitz, M.C. Ogilvie, R.L. Sugar, and D. Toussaint, in *Workshop on Fermion Algorithms*, edited by H. J. Hermann and F. Karsch, (World Scientific, Singapore, 1991).  
See also <http://physics.indiana.edu/~sg/milc.html>



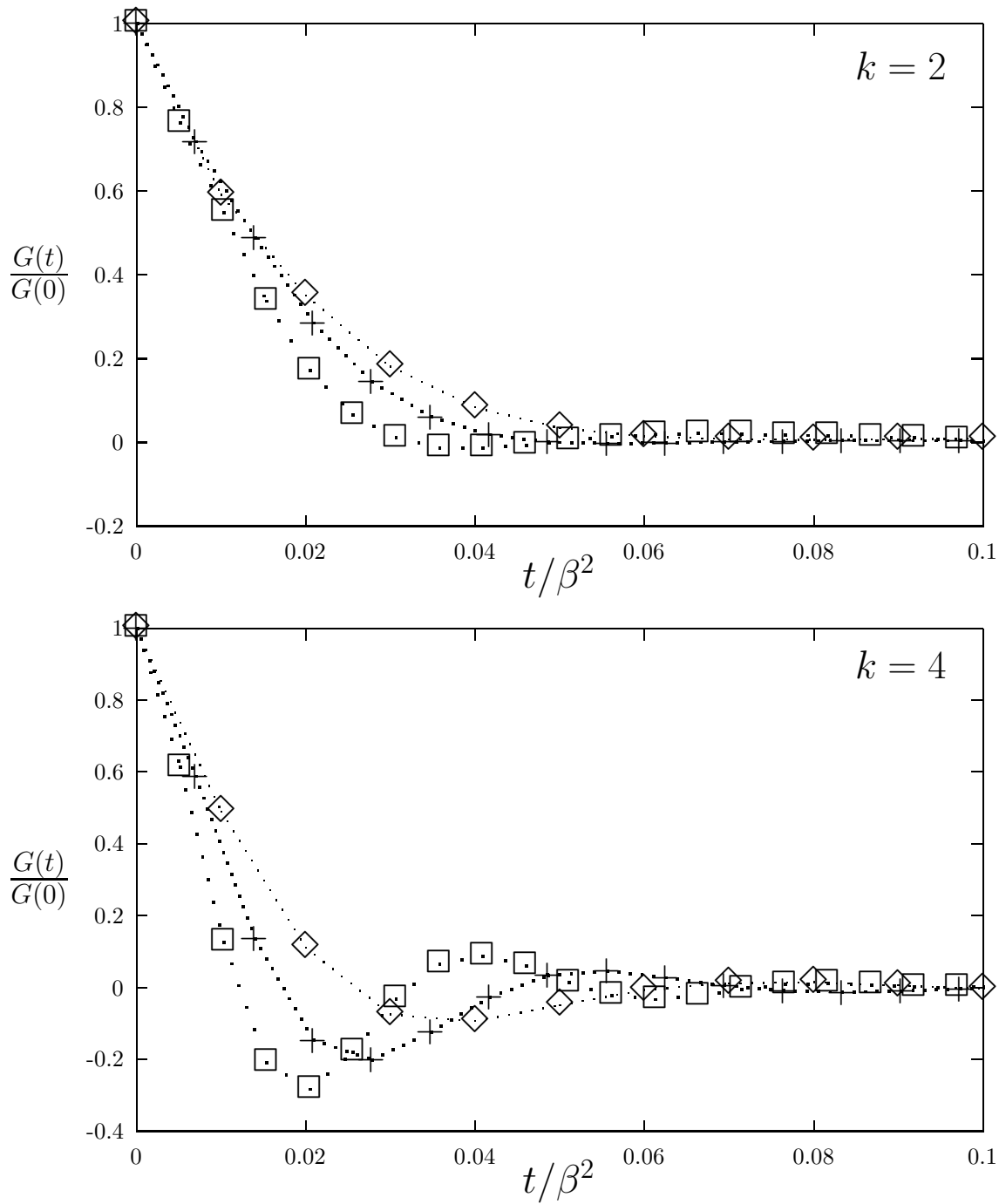


Figure 6: Real-time correlation functions  $G(k, t)$  of gauge fields in the Coulomb gauge plotted against  $t/\beta^2$ . The value of  $k$  is indicated on each plot. Each  $G(k, t)$  is normalized by its respective value at  $t = 0$ . Diamonds correspond to  $\beta = 10$ , plus signs to  $\beta = 12$  and squares to  $\beta = 14$  for a  $32^3$  lattice. In addition, the open circles in the  $k = 0$  plot show  $G(0, t)/G(0, 0)$  for  $\beta = 14$  on a  $14^3$  lattice. Wherever the errorbars are not shown, they are smaller than the plotting symbols.